PROCEEDINGS OF SCIENCE

X-ray Observation of Possible Cosmic-Ray Escaping Region of SNR G78.2+2.1

Dai Tateishi,[a,*] **Yuji Sunada,**[a] **Yukikatsu Terada**[a,b] **and Satoru Katsuda**[a]

[a] *Graduate School of Science and Engineering, Saitama University, 255 Shimo-Okubo, Sakura, Saitama, 338-8570, Japan*

[b] *Japan Aerospace Exploration Agency, Institute of Space and Astronautical Science, Sagamihara, Kanagawa, 252-5210, Japan*

E-mail: d.tateishi.919@ms.saitama-u.ac.jp

The observation of non-thermal radiation of SNRs are essential for elucidating the mechanism of particle acceleration. MAGIC and Fermi discovered very high energy (VHE) γ-ray radiation from the northern part of SNR G78.2+2.1 (MAGIC Collaboration. 2020). This radiation is suggested to be originated from cosmic rays escaping from the SNR. However, it is inconclusive since the electron energy distribution is not well estimated. To solve this problem, we analyzed data from the X-ray astronomy satellite Suzaku to evaluate the contribution of the leptonic emission of the broadband spectrum of MAGIC J2019+408. Our analysis revealed a hard X-ray component in the northern region of SNR G78.2+2.1 with a flux several times larger than the X-ray background radiation. The emission extending outside the SNR was represented in the X-ray image in 2-5 keV, but is not associated with the SNR. X-rays above 2 keV could be explained either by an absorbed thermal-emission model with a temperature of $1.6^{+0.4}_{-0.2}$ keV and low-solar ($0.3 \pm 0.2\,Z_{\odot}$) abundances or by an absorbed synchrotron ($\Gamma = 3.7 \pm 0.5$) radiation model with no statistically significant difference. From SED analysis of radio to VHE γ-ray, X-ray and γ-ray spectra can be reproduced by the synchrotron model with the magnetic field strength of 50 μG, but requires more-than one order-of-magnitude brighter radio flux than the observation result of the SNR shell. Alternatively, a magnetic intensity of 4 μG will also satisfy radio and VHE γ-ray flux, but this magnetic strength was significantly lower than what we expected for the diffusive shock acceleration. These results suggest that the observed X-rays have a different origin from non-thermal emission of MAGIC J2019+408, and some of the VHE γ-rays originated from escaped cosmic rays.

38th International Cosmic Ray Conference (ICRC2023)
26 July - 3 August, 2023
Nagoya, Japan

*Speaker

PoS(ICRC2023)268

1. Introduction

SNR G78.2+2.1 is a middle-aged (4-13 kyr [1–4]) shell-type supernova remnant (SNR) located 1.5-2.6 kpc [1–5] from Earth. Several telescopes have discovered very high energy (VHE) γ-rays from the northern part of the SNR. However, the radiative process and its distribution are still in debate. From VERITAS and Fermi/LAT analysis, [6] pointed out that the VHE γ-rays can be explained with a non-thermal bremsstrahlung model from the SNR shell, i.e., a leptonic model. Recently, MAGIC also observed this SNR and discovered the VHE γ-ray emission, MAGIC J2019+408, over the SNR shell and outward from the northern part of it [7]. However, in contrast to [6], the observed VHE γ-ray spectrum can be explained by pion decay, i.e., a hadronic model. Combined with the γ-ray distribution, they concluded that the VHE γ-rays most likely originated from the shell and the nearby molecular cloud that cosmic rays escaped from the SNR bombarded.

We focused on the fact that the energy distribution of non-thermal electrons are poorly evaluated, causing the uncertainty of the origin of the VHE γ-ray. In order to estimate the contribution of non-thermal emission from possible high-energy electrons (i.e., leptonic model), we performed the X-ray imaging spectroscopy. We utilized the X-ray observation performed by Suzaku/XIS [8] to search for the non-thermal X-ray emission associated with MAGIC J2019+408.

2. Observation and data reduction

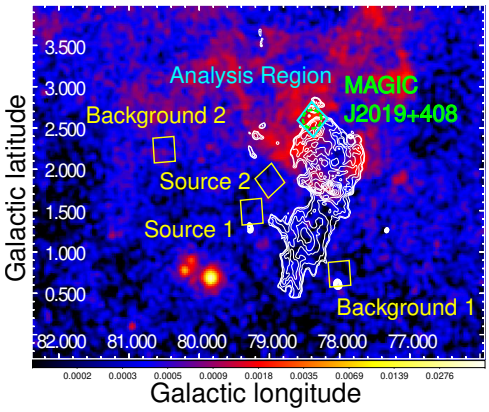

Figure 1: Position of Suzaku/XIS observations overlaid on the X-ray (0.4-2.4 keV) map observed by ROSAT/PSPC. The cyan box indicates the analyzed XIS FoV in this study, the green dashed circle indicates MAGIC J2019+408, and the white contour represents the 1420 MHz radio continuum observed by CGPS [9]. The yellow boxes indicate the XIS FoV analyzed by [10].

We analyzed Suzaku/XIS archival data (Obs. ID: 506017010, PI: Dr. Yasuyuki Tanaka, Energy range: 0.2-12 keV) observed on April 13, 2011 (Net exposure: 39 ks), aiming to probe the emission mechanism of the VHE γ-ray from the northern part of the SNR G78.2+2.1 discovered by Fermi/LAT [11] and VERITAS [12]. The position of the XIS field of view (FOV), MAGIC J2019+408, and radio shell of SNR G78.2+2.1 are shown in Figure 1. We used data products from Suzaku pipeline processing version 3.0.22.44 and the software package HEASoft[1] 6.28 [13] for the analysis.

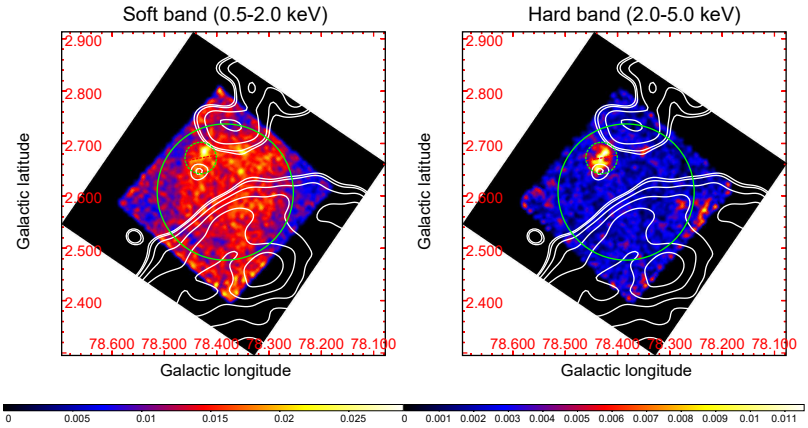

Figure 2: X-ray images of the northern region of SNR G78.2+2.1 observed by Suzaku/XIS. **Left**: X-ray image of the soft band (0.5–2.0 keV). **Right**: X-ray image of the hard band (2.0–5.0 keV). The white contour represents 1420 MHz radio continuum emission observed by CGPS [9].

3. Analysis and result

3.1 Image analysis

We extracted X-ray images from XIS1 and 3 within the energy range of soft (0.5-2.0 keV) and hard (2.0-5.0 keV) bands and subtracted the non-X-ray background (NXB) image. We ignored XIS0 image since there was an anomaly in the edge of the CCD. In addition, XIS2 was not operational due to the damage from a meteoroid strike. Vignetting was then corrected by dividing flat sky images created by `xissim` [14]. Finally, we merged the XIS1 and 3 images to improve the statistics and we detected $(4.72 \pm 0.03) \times 10^4$ and $(0.84 \pm 0.01) \times 10^4$ counts signals in the soft and hard band, respectively. The resultant flux images are shown in Figure 2. The white contour in Figure 2 represents 1420 MHz radio continuum emission observed by Canadian Galactic Plane Survey (CGPS) [9], which represents synchrotron radiation from SNR G78.2+2.1.

3.2 Spectral analysis

We extracted the spectrum from XIS0, 1, and 3, subtracted the NXB, and performed a spectral analysis as described below. We considered point-like sources, cosmic X-ray background (CXB), and Galactic X-ray background (GXB) presented in the X-ray background. We estimated their contribution using the following procedure.

3.2.1 Spectrum extraction and background estimation

We extracted the spectrum from the same region as MAGIC J2019+408, represented in the green circle in Figure 2. Since a point source was contaminated within our region of interest (ROI) (possibly related to NOMAD1 1309-0400043), we excluded it from the spectral extraction region. The NXB spectrum was obtained from the night Earth observation data using the `xisnxbgen` command and it was subtracted from the source spectrum.

[1]http://heasarc.gsfc.nasa.gov/ftools

To estimate the contribution of point-like sources, we analyzed Chandra/ACIS-I data (Obs. ID: 12676), which covered most of the source region. Using the `wavdetect` in CIAO (Ver. 4.14.0) [15], we detected 8 point-like sources with enough events to analyze in the ROI. We fitted the spectrum with an absorbed power-law model (TBabs × powerlaw), and the best-fit result was considered during the XIS analysis. The flux for the faintest point-like source in 2–10 keV was $\sim 2.38 \times 10^{-14}$ erg cm^{-2} s^{-1}. Comparing this value to the logN-logS plot in [16], we estimated the unresolved CXB flux to be $(4.0 \pm 0.3) \times 10^{-12}$ erg cm^{-2} s^{-1}. We modeled it with the canonical spectral model of CXB, i.e., absorbed power-law model (TBabs × powerlaw) with a photon index fixed to 1.4 [16] and considered it during the XIS analysis. The contribution of point-like sources and CXB were represented in the purple dot lines in Figure 3.

The GXB varies from place to place on the Galactic plane and strongly depends on the Galactic latitude. In order to estimate the GXB level of the ROI correctly, we surveyed the analysis result of XIS observations in the vicinity of the ROI. As a result, we noticed 4 XIS observations marked with yellow boxes in Figure 1. These regions were analyzed by [10], who pointed out that the observed X-rays are dominated by the GXB. We adopted the best-fit result of Background 2, closest to the Galactic latitude of the ROI, to the analysis.

3.2.2 Fitting and results

The resultant 2-8 keV NXB subtracted spectrum and the X-ray background (CXB, GXB) contribution to the spectrum are shown in Figure 3. We found that the flux of NXB subtracted spectrum exceeded 2–10 times that of the X-ray background. This result indicates that a component other than the X-ray background exists in the spectrum. In this study, we focus on the 2–8 keV component hereafter to evaluate the presence of non-thermal electrons. To investigate the radiation process of the excess spectrum, we first tested with a thermal plasma model (TBabs × APEC) and a non-thermal plasma model (TBabs × powerlaw). The best-fit results and parameters are shown in Figure 3 and Table 1, respectively. Comparing the reduced chi-squared value of each model, we could not find any statistically significant differences between them.

Table 1: Spectral-fit parameters

Thermal model			Non-thermal Model		
Model	Parameter	Value	Model	Parameter	Value
TBabs	$N_{\rm H}$ ($\times 10^{22}$ atoms cm^{-2})	$2.3^{+0.8}_{-0.9}$	TBabs	$N_{\rm H}$ ($\times 10^{22}$ atoms cm^{-2})	$3.2^{+1.2}_{-1.1}$
APEC	Plasma temperature (keV)	$1.6^{+0.4}_{-0.2}$	Power-law	Photon Index	3.7 ± 0.5
	Abundance ($Z/Z_{\odot}$)	0.3 ± 0.2		Norm. ($\times 10^{-2}$ @1 keV)	$4.6^{+5.0}_{-2.3}$
	EM ($\times 10^{56}$ cm^{-5} @1.7 kpc)	$1.3^{+0.7}_{-0.6}$		(photons keV^{-1} cm^{-2} s^{-1})	
	$\chi^2/d.o.f.$	485/501		$\chi^2/d.o.f.$	497/498

Note. The errors represent a 90% confidence level on an interesting single parameter.

4. Discussion

4.1 Origin and emission process of hard X-rays

Our image analysis revealed that soft band X-ray emission extends outside the SNR shell, which seems unrelated to the SNR. This spatial distribution is consistent with the large-scale structure

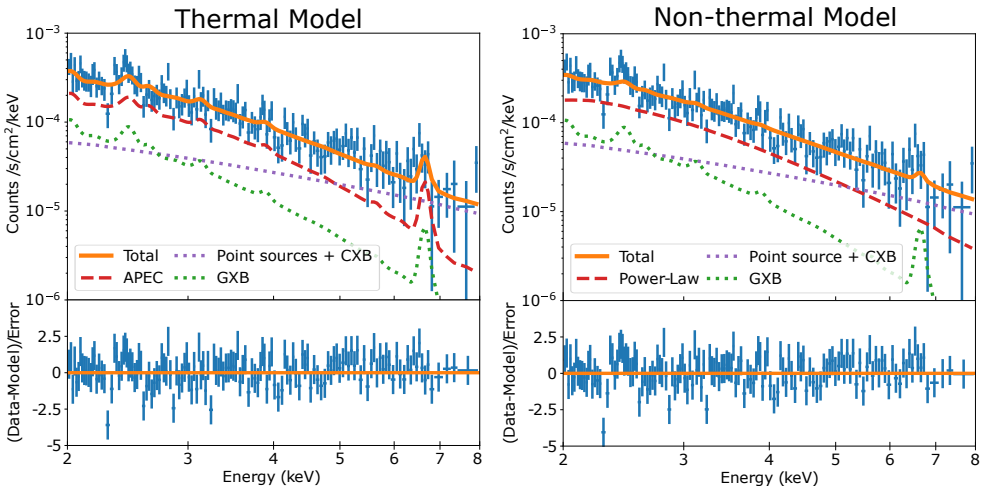

Figure 3: The best-fit results of XIS spectrum in thermal (left figure) and non-thermal (right figure) models. The blue lines represent NXB subtracted spectrum, while the green and purple dot lines represent GXB and point-like sources + CXB, respectively. The red dashed lines represent thermal or non-thermal components. The orange lines represent the total best-fit model obtained from the thermal or the non-thermal model.

shown with the ROSAT/PSPC observations (0.4-2.4 keV) in Figure 1. In contrast to the soft band, the hard band X-ray emission was distributed uniformly in the XIS FoV and did not align with the radio shell of the SNR. This result suggests that the hard X-rays have no relation to the SNR. In addition, the spatial distribution of hard X-ray does not match the distribution of the radio continuum (325, 408 GHz) [17, 18], HI emission [9], nor CO cloud [19]. No further information on the origin of the hard X-rays was obtained from the imaging analysis beyond the hard X-rays are not associated with the SNR.

The observed energy spectrum can be well described with both thermal and non-thermal models (Section 3.2), but with no statistically significant differences. To test the validity of the thermal model, we calculated the electron density from the emission measure (EM). Assuming that the thermal emission originated from a cylindrical object with a radius of 0.13° (≈ 3.86 pc @1.7 kpc), electron to proton ratio of 1, the filling factor of f, and the depth of h, the electron density will be $(0.16 \pm 0.04) f^{-1/2} (h/3.86\,\mathrm{pc})^{-1/2}\,\mathrm{cm}^{-3}$. This density is comparable with the ISM density [20]. It is notable that the depth h may be larger than the 3.86 pc, thus the density may be smaller than this value. In addition, the electron temperature, hydrogen column density, and chemical abundances of the thermal model are reasonably consistent with those of the high-temperature component of [10], representing GXB. These results strongly suggest that the hard X-ray observed with the XIS is the thermal emission localized to the Cygnus region spread uncorrelated with the SNR.

On the other hand, the photon index of the non-thermal model is softer than that expected from diffusive shock acceleration in the SNR shock. Such a soft index could be explained by non-thermal emission from electrons which have higher energy than the cut-off energy. Alternatively, non-thermal bremsstrahlung may also be considered as a radiation mechanism. However, assuming the particle index of 2, which is expected by the diffusive shock acceleration in the shock region of the SNR, the expected photon index of non-thermal bremsstrahlung is ≈ 1 [21], inconsistent with the best-fit result. This result does not support the non-thermal bremsstrahlung scenario mentioned

in [3], in which harder X-ray spectra are reported. The reason for this inconsistency may come from the difference of the treatment of the local background model in the analysis.

4.2 Emission process of MAGIC J2019+408

We performed the spectral energy distribution (SED) analysis to evaluate the contribution of the emission by the leptonic scenario of the broadband spectrum of MAGIC J2019+408. We tested purely leptonic one-zone models consistent with synchrotron emission in the radio to X-ray band and inverse Compton emission in VHE γ-ray, with the following two situations; 1) X-rays are fully reproduced by the synchrotron emission, or 2) X-rays have a different origin from synchrotron emission, for example, local thermal emission, etc. In scenario 1, X-rays and VHE γ-rays could be explained simultaneously by the leptonic model with the magnetic field strength of 50 μG, as shown in Figure 4 and Table 2. However, this scenario required at least 10 times higher radio flux than the radio observation of the SNR rim, inconsistent with the radio observation result. In scenario 2, we treated the X-ray as an upper limit of non-thermal X-rays and radio of MAGIC J2019+408, respectively. As a result, the broadband SED could be reproduced by the leptonic model with the magnetic field strength of 4 μG, as shown in Figure 4 and Table 2. However, there is no good interpretation of how and where the electrons accelerated in such a low magnetic field via diffusive shock acceleration. In summary, a one-zone purely leptonic scenario failed to explain the radio, X-ray, and VHE γ-ray emission simultaneously. Therefore, we conclude that some of the VHE γ-rays originated from cosmic rays, i.e., a hadronic origin. In addition, this result suggests that the observed X-rays originated from thermal plasma as indicated by the X-ray imaging analysis, or non-thermal plasma which has no relation to MAGIC J2019+408.

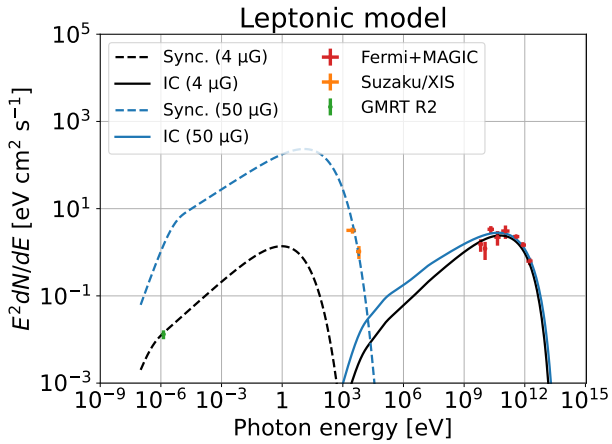

Figure 4: Broad-band SED with models for which the γ-ray emission is inverse Compton, i.e. a leptonic model. The orange lines, red lines, and green dot represent the X-ray spectrum detected by XIS, the γ-ray spectrum detected by Fermi/LAT and MAGIC [7], and 325 MHz radio flux in region R2 observed by GMRT [17], respectively. The dot line and black line represent the synchrotron and inverse Compton model of scenario 1 (black) and scenario 2 (blue).

5. Conclusion

We analyzed Suzaku/XIS data to evaluate the contribution of the leptonic emission of the broadband spectrum of MAGIC J2019+408. From spectrum analysis, we discovered X-rays that exceeded 2–10 times that of the X-ray background (CXB and GXB), from ROI. The X-ray distribution of the hard band did not correlate with the structures of MAGIC J2019+408, the SNR shell, HI emission, and CO cloud. The X-ray spectrum can be well described with either the thermal

Table 2: Parameters of SED in Figure 4

Parameter	Value	Parameter	Value
2.72 K CMBR density (eV cm^{-3})	0.261	Electron density of scenario 1 ($\times 10^{34}$ eV^{-1})	3.0
30 K FIR density (eV cm^{-3})	0.5	Electron cut-off energy of scenario 1 (TeV)	2.8
3000 K NIR density (eV cm^{-3})	1.0	Electron density of scenario 2 ($\times 10^{34}$ eV^{-1})	3.0
Particle index (4 μG)	2.4	Electron cut-off energy of scenario 2 (TeV)	2.4
Particle index (50 μG)	2.0	Distance to the SNR (kpc)	1.7

or non-thermal models; no statistically significant differences existed between them. The best-fit parameter of the thermal model was within the error of the GXE model in [10]. This result suggests that the hard X-rays is local emission that spread uncorrelated with the SNR. In contrast, the photon index of the non-thermal model can be described by synchrotron emission from a power-law electron energy distribution in the higher energy band of an exponential cut-off. This result does not support the non-thermal bremsstrahlung scenario mentioned in [3]. From the SED analysis, the one-zone all-leptonic scenario could not explain the spectrum from radio to VHE γ-ray with reasonable physical conditions of acceleration. These results suggest that the observed X-rays have different origin from the non-thermal emission of MAGIC J2019+408 and some of the γ-rays are of hadronic origin.

References

[1] L.A. Higgs, T.L. Landecker and R.S. Roger, *The true extent of the gamma Cygni supernova remnant.*, **82** (1977) 718.

[2] T.A. Lozinskaya, V.V. Pravdikova and A.V. Finoguenov, *The Supernova Remnant G78.2+2.1: New Optical and X-ray Observations*, *Astronomy Letters* **26** (2000) 77.

[3] Y. Uchiyama, T. Takahashi, F.A. Aharonian and J.R. Mattox, *ASCA View of the Supernova Remnant γ Cygni (G78.2+2.1): Bremsstrahlung X-Ray Spectrum from Loss-flattened Electron Distribution*, **571** (2002) 866 [astro-ph/0202414].

[4] D.A. Leahy, K. Green and S. Ranasinghe, *X-ray and radio observations of the γ Cygni supernova remnant G78.2+2.1*, **436** (2013) 968 [1307.3151].

[5] T.L. Landecker, R.S. Roger and L.A. Higgs, *Atomic hydrogen in a field in Cygnus X containing the supernova remnant G78.2+2.1.*, **39** (1980) 133.

[6] G. Piano, M. Cardillo, M. Pilia, A. Trois, A. Giuliani, A. Bulgarelli et al., *AGILE Study of the Gamma-Ray Emission from the SNR G78.2+2.1 (Gamma Cygni)*, **878** (2019) 54 [1905.01255].

[7] MAGIC Collaboration, V.A. Acciari, S. Ansoldi, L.A. Antonelli, A. Arbet Engels, D. Baack et al., *Study of the GeV to TeV morphology of the γ Cygni SNR (G 78.2+2.1) with MAGIC and Fermi-LAT. Evidence for cosmic ray escape*, **670** (2023) A8 [2010.15854].

[8] K. Mitsuda, M. Bautz, H. Inoue, R.L. Kelley, K. Koyama, H. Kunieda et al., *The X-Ray Observatory Suzaku*, **59** (2007) S1.

[9] A.R. Taylor, S.J. Gibson, M. Peracaula, P.G. Martin, T.L. Landecker, C.M. Brunt et al., *The Canadian Galactic Plane Survey*, **125** (2003) 3145.

[10] T. Mizuno, T. Tanabe, H. Takahashi, K. Hayashi, R. Yamazaki, I. Grenier et al., *Suzaku Observation of the Fermi Cygnus Cocoon: The Search for a Signature of Young Cosmic-Ray Electrons*, **803** (2015) 74 [1502.01390].

[11] A.A. Abdo, M. Ackermann, M. Ajello, A. Allafort, E. Antolini, W.B. Atwood et al., *Fermi Large Area Telescope First Source Catalog*, **188** (2010) 405 [1002.2280].

[12] A. Weinstein, *The VERITAS Survey of the Cygnus Region of the Galactic Plane*, *arXiv e-prints* (2009) arXiv:0912.4492 [0912.4492].

[13] Nasa High Energy Astrophysics Science Archive Research Center (Heasarc), "HEAsoft: Unified Release of FTOOLS and XANADU." Astrophysics Source Code Library, record ascl:1408.004, Aug., 2014.

[14] Y. Ishisaki, Y. Maeda, R. Fujimoto, M. Ozaki, K. Ebisawa, T. Takahashi et al., *Monte Carlo Simulator and Ancillary Response Generator of Suzaku XRT/XIS System for Spatially Extended Source Analysis*, **59** (2007) 113 [astro-ph/0610118].

[15] A. Fruscione, J.C. McDowell, G.E. Allen, N.S. Brickhouse, D.J. Burke, J.E. Davis et al., *CIAO: Chandra's data analysis system*, in *Society of Photo-Optical Instrumentation Engineers (SPIE) Conference Series*, D.R. Silva and R.E. Doxsey, eds., vol. 6270 of *Society of Photo-Optical Instrumentation Engineers (SPIE) Conference Series*, p. 62701V, June, 2006, DOI.

[16] A. Moretti, S. Campana, D. Lazzati and G. Tagliaferri, *The Resolved Fraction of the Cosmic X-Ray Background*, **588** (2003) 696 [astro-ph/0301555].

[17] J.M. Paredes, P. Benaglia, C.H. Ishwara-Chandra, V. Bosch-Ramon and M. Strzys, *Exploring the region encompassing γ Cygni SNR and MAGIC J2019+408 with the GMRT at 325 and 610 MHz*, **660** (2022) A73 [2203.06427].

[18] Y. Ladouceur and S. Pineault, *New perspectives on the supernova remnant G78.2+2.1*, **490** (2008) 197.

[19] D.J. Schlegel, D.P. Finkbeiner and M. Davis, *Maps of Dust Infrared Emission for Use in Estimation of Reddening and Cosmic Microwave Background Radiation Foregrounds*, **500** (1998) 525 [astro-ph/9710327].

[20] E.M. Berkhuijsen and A. Fletcher, *Density probability distribution functions of diffuse gas in the Milky Way*, **390** (2008) L19 [0806.4316].

[21] J. Vink, *Physics and Evolution of Supernova Remnants* (2020), 10.1007/978-3-030-55231-2.